THE UNIVERSITY OF READING

Linearising the Kepler Problem for 4D-Var Data Assimilation

by

Laura Stanton

Numerical Analysis Report 3/2002

DEPARTMENT OF MATHEMATICS

Linearising the Kepler Problem

For 4D-Var Data Assimilation

Laura Stanton

MSc MNMAO

University of Reading

August 2002

I confirm that this is my own work, and the use of all material from other sources has been properly and fully acknowledged.

Laura Stanton

Acknowledgements

Completing this dissertation would not have been possible without the help and support of my supervisors, Amos Lawless and Ian Roulstone. I also wish to thank Nancy Nichols for her input at the start of the summer.

Thanks are also due to NERC for providing the financial support without which I would have been unable to do the course.

I'm also grateful to the staff of the maths department, in particular Sue Davis who has looked after us all so well this year. I'd like to thank my fellow MSc students, especially Matt and Sarah, who have helped make it such an enjoyable time.

I would like to say thanks to my parents, who are still supportive and uncomplaining, even in my fifth year as a student.

Last but definitely not least, I'd like to thank my fiancé Luke who has kept me sane this year, and looked after me even in my worst moods.

Abstract

We aim to investigate the preliminary stages of setting up a 4D-Var data assimilation scheme for the Kepler problem. We investigate the dynamics of the system and set up a non-linear model to describe the motion using the Störmer-Verlet method. Tests prove the scheme is a good choice for the problem. We use this to produce a tangent linear model, the code for this is tested and shown to be a correct linearisation. We test the conservation properties of the linear model, thus demonstrating the possible viability of a 4D-Var scheme.

Contents

1 Introduction **5**

1.1 Chapter Outline 6

2 The Kepler Problem **8**

2.1 Kepler's Three Laws 8

2.1.1 The Ellipse 9

2.1.2 Equal Areas in Equal Time 10

2.1.3 Period-Radius Relation 13

2.2 The Equations of Motion 13

2.3 Conservation Properties 15

3 Numerical Scheme **16**

3.1 Hamiltonian Systems 16

3.2 Numerical Scheme 17

3.2.1 Testing the Model 21

3.2.2 Testing the Sensitivity 23

4 Linearising Kepler's Problem **26**

4.1 4D-Var Data Assimilation 26

4.1.1 Causality 28

4.1.2 Tangent Linear Hypothesis 29
4.2 The Linear Model 29
4.2.1 Testing the Linear Model 32

5 Numerical Experiments **37**
5.1 Validity 37
5.2 Conservation Properties 42

6 Conclusion **51**

List of Figures

2.1 Illustration of polar coordinates, taken from [1] 11

2.2 Illustration of Kepler's second law, taken from [1] 12

3.1 Comparison of Numerical Methods for the Kepler Problem, taken from [3] 18

3.2 Trajectories of the orbitting body 20

3.3 Behaviour of energy and angular momentum in the model . . 22

3.4 Energy versus time, $h = 0.001$, eccentricity= 0.5 23

3.5 Graphs to show sensitivity to initial conditions for different eccentricities; a, $e = 0$; b, $e = 0.5$; c, $e = 0.9$ 25

4.1 Graphs to Illustrate Correctness for Various Eccentricities . . 34

4.2 Graphs to Illustrate Correctness for Various Run Times 35

5.1 Evolution of the Q_1 perturbation for the non-linear and linear models, for different γ ($h = 0.001$, $e = 0$, $\gamma = 0.1, 0.01, 0.001$) . 39

5.2 Evolution of the Q_1 perturbation for the non-linear and linear models, for different eccentricities ($h = 0.001$, $\gamma = 0.01$, $e = 0, 0.5, 0.9$) 40

5.3 Evolution of the P_1 perturbation for the non-linear and linear models, for different γ ($h = 0.001$, $e = 0$, $\gamma = 0.01$) 41
5.4 Non-linear and linear expressions for the energy, $h = 0.001$, $e = 0$, $\gamma = 0.001$ 44
5.5 Non-linear and linear expressions for the energy, $h = 0.001$, $e = 0.5$, $\gamma = 0.001$ 45
5.6 Non-linear and linear expressions for the energy, $h = 0.001$, $e = 0.9$, $\gamma = 0.001$ 46
5.7 Non-linear and linear expressions for the energy, $h = 0.001$, $e = 0.9$, $\gamma = 0.001$ 47
5.8 Non-linear and linear expressions for the angular momentum, $h = 0.001$, $e = 0.5$, $\gamma = 0.001$ 49

Chapter 1

Introduction

4D variational data assimilation is a technique often applied in meteorology and oceanography, including numerical weather prediction [4, 5, 10]. It incorporates observational data into a model over a given time interval and at the same time satisfies a dynamical constraint. We shall be investigating a system that is numerically easier than numerical weather prediction - Kepler's problem. This describes the motion of two bodies due to their gravitational pull on each other. We will consider here the early stages of setting up such a problem, and look at the effects the model has on the global properties of the system.

4D-Var involves the minimisation of a *cost function*, using the model equations as constraints [7]. This function is a measure of the distance between the model state and the observations, and the model state and the background. The minimum is thus the model solution which most closely fits the observational data, whilst staying close to the background state. The first step in finding this cost function and solving the minimisation problem is to

create a *tangent-linear* model which describes the evolution, to first order, of a perturbation δx in the vicinity of trajectory $x(t)$. It is the aim of this project to set up such a model.

To do this we first require a non-linear model which accurately describes the behaviour of an orbitting body, and most importantly displays the same physical characteristics as the real system. This is then linearised about $\bar{\mathbf{x}}$, where $\bar{\mathbf{x}}$ is a solution of the non-linear system. We usually use an *incremental* form of 4D-Var that directly uses tangent linear model [?]. It is the behaviour of these perturbations that we shall be looking at in this project. Once the linearisation has been achieved, we shall look at how well the linear model retains the global features of the continuous problem, such as conservation properties. This information is important as one may wish to use conservation laws as constraint equations for the 4D-Var assimilation.

1.1 Chapter Outline

- Chapter 2: This chapter looks at the laws of Kepler, and the physics behind them. It also includes the equations of motion that describe the dynamics of the system.
- Chapter 3: Here we shall look at the numerical scheme that will be used to produce the *non-linear* model. This model will then be tested to see if it retains the global features of the problem.

- Chapter 4: This discusses some of the theory behind variational data assimilation, and explains how the model is linearised. It also includes tests of the linearised code.
- Chapter 5: Here we carry out some tests on the validity of the linearisation, and whether the conservation laws can be used as constraint equations.
- Chapter 6: Summarises the results of the project.

Chapter 2

The Kepler Problem

In this chapter, we shall list the three laws of Kepler and look at each in detail. We shall then go on to look at the equations governing the motion as a result of these laws, and look at the conservation properties of the problem.

2.1 Kepler's Three Laws

In the early seventeenth century, following detailed observations and analysis of the planetary motion within our solar system, Johannes Kepler deduced his three laws relating to the motion of each planet around the sun.

- The planets follow an elliptical orbit, with the sun at one focus.
- A line from the planet to the sun will sweep out equal areas in equal times.
- The square of the period of the orbit is proportional to the cube of its semi-major axis.

These laws describe a system that is often referred to as the two-body problem. They govern the motion of two bodies that attract each other, neglecting the effects of any other bodies in the system. This simplifies the problem greatly as the adddition of a third attracting body can lead to extremely complex motion.

For the purposes of this project, the problem will be further simplified. This is done by choosing a coordinate system such that one of the bodies is fixed at the centre, so that the motion remains in one plane. The system will also be non-dimensionalised, as will be shown later in this chapter.

The material in these sections follows the argument given in Chapter 6 of David Acheson's book, *From Calculus to Chaos* [1].

2.1.1 The Ellipse

To begin we shall look at the first law, and the equation that describes the path of an ellipse in the $x - y$ plane,

$$\frac{x^2}{a^2} + \frac{y^2}{b^2} = 1. \tag{2.1}$$

Here a and b are the semi-major and semi-minor axes of the ellipse respectively and are constants. From this it can be seen that a special case of the ellipse occurs when $a = b$, this gives the equation for a circle. We can assume that $b \leq a$. Typically the ellipse is described by its *eccentricity*, e, given by the following formula

$$e = \left(1 - \frac{b^2}{a^2}\right)^{\frac{1}{2}} \tag{2.2}$$

This measures how 'squashed' the ellipse is. We can see that if the eccentricity is set to zero, then $a = b$ and the ellipse becomes a circle. The eccentricity also tells us the position of the focal points which are at $(\pm ae, 0)$. The greater the eccentricity, the more off-centred the focal points are.

2.1.2 Equal Areas in Equal Time

The second of Kepler's laws arises from the fact that there is a central force. To see this, we must look at the equations of motion. For ease of discussion, we will use polar coordinates, (r, θ), although later, for the numerical scheme, it will prove more straightforward to use Cartesian coordinates. Although we know that gravitational attraction obeys an inverse-square law, the law of equal areas is true for *any* central force, so it is this general case that we shall look at.

To obtain the equations of motion, we need to split the velocity and acceleration into a radial component (away from the centre) and a transverse component (at a tangent to the radial direction), as shown in figure 2.1. We can consider this to be in the complex plane, therefore the position of the body is $z = x + iy$ or $z = re^{i\theta}$. To get the velocity components we differentiate with respect to time,

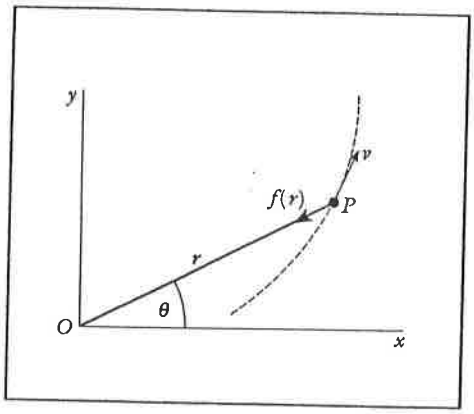

Figure 2.1: Illustration of polar coordinates, taken from [1]

$$\frac{\mathrm{d}z}{\mathrm{d}t} = \frac{\mathrm{d}r}{\mathrm{d}t}e^{i\theta} + ir\frac{\mathrm{d}\theta}{\mathrm{d}t}e^{i\theta} \tag{2.3}$$

$$= \frac{\mathrm{d}r}{\mathrm{d}t}e^{i\theta} + r\frac{\mathrm{d}\theta}{\mathrm{d}t}e^{i(\theta+\frac{\pi}{2})} \tag{2.4}$$

giving radial and transverse velocity components $(\frac{\mathrm{d}r}{\mathrm{d}t}, r\frac{\mathrm{d}\theta}{\mathrm{d}t})$. To find the acceleration components we need to differentiate (2.3). The resulting components are $(\frac{\mathrm{d}^2r}{\mathrm{d}t^2} - r\left(\frac{\mathrm{d}\theta}{\mathrm{d}t}\right)^2, 2\frac{\mathrm{d}r}{\mathrm{d}t}\frac{\mathrm{d}\theta}{\mathrm{d}t} + r\frac{\mathrm{d}^2\theta}{\mathrm{d}t^2})$. Now using Newton's second law, and by considering that the force in the radial direction, $f(r)$, is *towards* the centre, and that there is no tangential force, we obtain the following equations

$$m\left(\frac{\mathrm{d}^2r}{\mathrm{d}t^2} - r\left(\frac{\mathrm{d}\theta}{\mathrm{d}t}\right)^2\right) = -f(r), \tag{2.5}$$

$$m\left(2\frac{\mathrm{d}r}{\mathrm{d}t}\frac{\mathrm{d}\theta}{\mathrm{d}t} + r\frac{\mathrm{d}^2\theta}{\mathrm{d}t^2}\right) = 0. \tag{2.6}$$

To arrive at Kepler's second law we need to first multiply (2.6) by r,

$$2r\frac{\mathrm{d}r}{\mathrm{d}t}\frac{\mathrm{d}\theta}{\mathrm{d}t} + r^2\frac{\mathrm{d}^2\theta}{\mathrm{d}t^2} = 0. \tag{2.7}$$

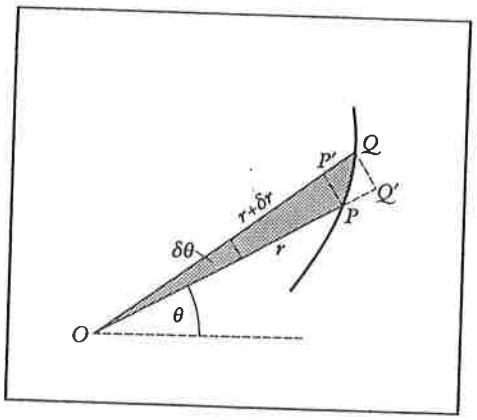

Figure 2.2: Illustration of Kepler's second law, taken from [1]

The left hand side is the derivative of $r^2\dot{\theta}$, therefore as the derivative is zero, this implies that

$$r^2\frac{\mathrm{d}\theta}{\mathrm{d}t} = \text{constant}. \tag{2.8}$$

Now consider figure 2.2. The area swept out is bounded below by sector OPP' and above by OQQ', giving the following inequality for the area

$$\frac{1}{2}r^2\delta\theta < \delta A < \frac{1}{2}(r+\delta r)^2\delta\theta. \tag{2.9}$$

We divide by δt and allow all the δ terms tend to zero. Both sides of the inequality then tend to $\frac{1}{2}r^2\dot{\theta}$, and we have

$$\frac{\mathrm{d}A}{\mathrm{d}t} = \frac{1}{2}r^2\frac{\mathrm{d}\theta}{\mathrm{d}t}. \tag{2.10}$$

By comparison with (2.8) we can see that the rate of change of area is constant, i.e. the line OP sweeps out areas at a constant rate.

2.1.3 Period-Radius Relation

The third law, states that $T_o^2 \propto a^3$, where T_o is the period of the orbit and a is the semi-major axis as defined previously. This arises from the fact that the gravitational attraction is an inverse-square law.

$$F(r) = \frac{GMm}{r^2} \tag{2.11}$$

Here G is the universal gravitational constant, M the mass of the central body, m the mass of the orbitting body, and r the distance between the two bodies. For simplicity we assume that we have a circular orbit. The period is thus $\frac{2\pi r}{v}$, where v is the tangential velocity, also the centripetal force is $\frac{mv^2}{r}$. By comparison of this with (2.11), and some manipulation we find

$$T = 2\pi \left(\frac{r^3}{GM}\right)^{\frac{1}{2}}. \tag{2.12}$$

It can be shown that this also holds for the more general case of an ellipse, where the radius, r, is replaced by the semi-major axis, a (see pages 78 to 81 of Acheson's text [1]).

2.2 The Equations of Motion

However, for modelling purposes it is simpler to consider the problem in Cartesian coordinates, resolving the force towards the origin. Consider equations (2.4) and (2.5) which we arrived at by resolving the velocity and acceleration into radial and transverse components. If we instead use (x, y) coordinates and set $f(r) = \frac{GMm}{r^2}$, we resolve the force towards the origin into a component $\frac{GMmx}{r^3}$ in the negative x direction, and a component $\frac{GMmy}{r^3}$

in the negative y direction. As $r = (x^2 + y^2)^{\frac{1}{2}}$, we then have the following equations of motion,

$$\frac{\mathrm{d}\mathbf{q}}{\mathrm{d}t} = \frac{\mathbf{p}}{m} \tag{2.13}$$

$$\frac{\mathrm{d}\mathbf{p}}{\mathrm{d}t} = -\frac{GM\mathbf{q}}{(q_1^2 + q_2^2)^{\frac{3}{2}}} \tag{2.14}$$

where $(q_1, q_2) = (x, y)$, and $\mathbf{p}$ is the momentum of the orbitting body.

To further simplify the problem, we can introduce non-dimensional variables. By choosing $\tilde{\mathbf{q}} = \frac{\mathbf{q}}{d}$ (thus $\tilde{\mathbf{p}} = \frac{\mathbf{p}}{d}$), and $\tilde{t} = \left(\frac{GM}{d^3}\right)^{\frac{1}{2}} t$, where d is the distance to the origin at $t = 0$, we get the following equations,

$$\frac{\mathrm{d}\tilde{\mathbf{q}}}{\mathrm{d}t} = \tilde{\mathbf{p}} \tag{2.15}$$

$$\frac{\mathrm{d}\tilde{\mathbf{p}}}{\mathrm{d}t} = -\frac{\tilde{\mathbf{q}}}{(\tilde{q}_1^2 + \tilde{q}_2^2)^{\frac{3}{2}}}, \tag{2.16}$$

where $\tilde{\mathbf{q}}$ and $\tilde{\mathbf{p}}$ are the non-dimensionalised position and momentum vectors respectively. This means that distances are measured in units of d, while time is in units of $\left(\frac{d^3}{GM}\right)^{\frac{1}{2}}$. It is these final equations that will be used to produce a model of the Kepler problem. From now on we shall drop the tilde for clarity, and whenever we refer to position, momentum, distance and time, it is in this dimensionless form.

2.3 Conservation Properties

It is also important to note that this problem has conserved quantities. The two-body problem conserves both total energy and angular momentum following the motion [8]. This characteristic is intrinsic to the physical problem, and will provide a useful test of the discretised equations. The expression for the total enegy is the sum of the kinetic energy and the potential energy, in its non-dimensionalised form this is given by,

$$E = \frac{1}{2}\left(p_1^2 + p_2^2\right) - \frac{1}{q_1^2 + q_2^2)^{\frac{1}{2}}} = \text{constant}. \tag{2.17}$$

The angular momentum is given by

$$L = q_1 p_2 - p_1 q_2 = \text{constant}. \tag{2.18}$$

Chapter 3

Numerical Scheme

When considering which scheme to use we are usually concerned with finding one that is not only stable, but also minimises the local truncation error arising from the discretisation, i.e. more accurate. However such methods, although locally accurate, do not always account for the global features of the system. Section 2.3 showed that intrinsic to the Kepler problem is the fact that *energy is conserved*, thus it is essential that the model captures this property. This can be illustrated by considering the effect of energy loss in a model of the two-body problem [3]. The orbitting body would spiral inwards, which is physically incorrect - planets do not spiral into the sun. Hence for this problem accuracy is less important than the conservation properties.

3.1 Hamiltonian Systems

The Kepler problem is one example of a Hamiltonian system. Such systems have a conserved quantity, the *Hamiltonian*. As discussed in section 2.3, for

the Kepler problem this is the total energy, i.e. the sum of the kinetic and potential energies.

$$H = \frac{1}{2}\left(p_1^2 + p_2^2\right) - \frac{1}{(q_1^2 + q_2^2)^{\frac{1}{2}}} = E = \text{constant.} \tag{3.1}$$

In addition to this, due to the central nature of the force, *angular momentum* is conserved.

In recent years, the growth of *geometric integration* [3, 8] has attempted to address the issue of preserving global features, and has produced numerical methods which incorporate the physical constraints of the original problem. For the two-body problem it is the underlying *conservation laws* that are important. In other examples, it may be the symmetry of the problem, or perhaps asymptotic behaviour that dictates the evolution. One set of geometric methods applied to Hamiltonian problems are particularly good at conserving energy, and can also conserve angular momentum, these are known as *symplectic methods* [3]. Because of this we will use a symplectic method to model the two-body problem.

3.2 Numerical Scheme

Following previous work on the Kepler problem [3, 8, 13], we will use the Störmer-Verlet method. This scheme was first used in the field of molecular dynamics, and has frequently been used to model Hamiltonian systems. The diagram below, taken from the paper by Budd and Piggott [3] illustrates how well this method behaves, in comparison with the forward Euler and

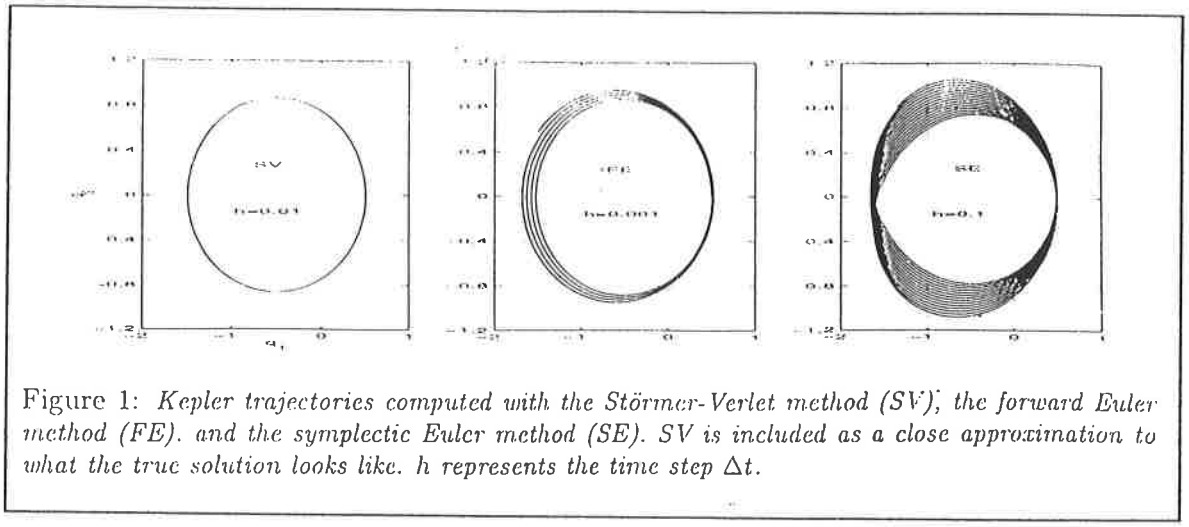

Figure 1: *Kepler trajectories computed with the Störmer-Verlet method (SV), the forward Euler method (FE), and the symplectic Euler method (SE). SV is included as a close approximation to what the true solution looks like. h represents the time step Δt.*

Figure 3.1: Comparison of Numerical Methods for the Kepler Problem, taken from [3]

symplectic Euler methods. We see that the Störmer-Verlet scheme gives a more accurate representation of the orbit and more closely follows the path of the ellipse during each orbit. This is a symplectic Runge-Kutta method, and is second order accurate. A higher order symplectic method could have been chosen. This would have given more accurate results [11, 12], however it is the global properties that are of most interest here and local accuracy is less important. As this second order method retains the global properties, we shall use this scheme as it is simpler to code. The method is taken from a 1994 paper by Skeel and Biesiadecki [13], and approximates the following set of continuous equations.

$$\frac{\mathbf{dp}}{\mathbf{d}t} = \mathbf{F} \tag{3.2}$$

$$\frac{\mathbf{dq}}{\mathbf{d}t} = \frac{\mathbf{p}}{m} \tag{3.3}$$

The discretised equations are

$$\mathbf{P}_{n+\frac{1}{2}} = \mathbf{P}_n + \frac{h}{2}\mathbf{F}_n \tag{3.4}$$

$$\mathbf{Q}_{n+1} = \mathbf{Q}_n + hm^{-1}\mathbf{P}_{n+\frac{1}{2}} \tag{3.5}$$

$$\mathbf{F}_{n+1} = \mathbf{F}(\mathbf{Q}_{n+1}) \tag{3.6}$$

$$\mathbf{P}_{n+1} = \mathbf{P}_{n+\frac{1}{2}} + \frac{h}{2}\mathbf{F}_{n+1} \tag{3.7}$$

Here $\mathbf{P}$ is the approximated momentum vector, $\mathbf{Q}$ the approximated position vector, and n indicates the n^{th} time level. $\mathbf{F}$ is the function that describes the evolution of the momentum, and is specific to the problem.

For our model $\mathbf{F}(\mathbf{Q}) = \frac{\mathbf{Q}}{(Q_1^2+Q_2^2)^{\frac{3}{2}}}$. Using this, and recalling that the model is dimensionless, i.e here the masses are unity, we have our model equations.

$$\mathbf{P}_{n+\frac{1}{2}} = \mathbf{P}_n + \frac{h}{2}\frac{\mathbf{Q}_n}{(Q_{1n}^2 + Q_{2n}^2)^{\frac{3}{2}}} \tag{3.8}$$

$$\mathbf{Q}_{n+1} = \mathbf{Q}_n + h\mathbf{P}_{n+\frac{1}{2}} \tag{3.9}$$

$$\mathbf{F}_{n+1} = \frac{\mathbf{Q}_{n+1}}{(Q_{1n+1}^2 + Q_{2n+1}^2)^{\frac{3}{2}}} \tag{3.10}$$

$$\mathbf{P}_{n+1} = \mathbf{P}_{n+\frac{1}{2}} + \frac{h}{2}\mathbf{F}_{n+1} \tag{3.11}$$

These equations are then put into code. For our numerical experiments, we begin by using the following initial conditions, these describe the body starting from the perihelion - the point of closest approach. The resulting

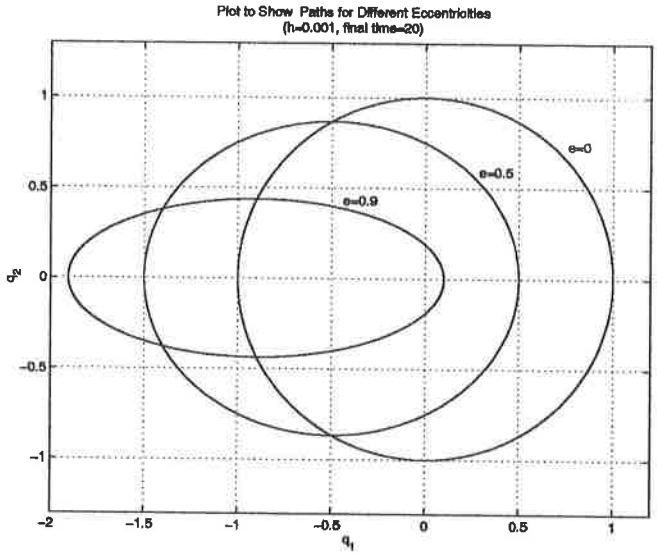

Figure 3.2: Trajectories of the orbitting body

orbit then has a period of 2π.

$$q_1 = 1 - e \tag{3.12}$$

$$q_2 = 0 \tag{3.13}$$

$$p_1 = 0 \tag{3.14}$$

$$p_2 = \sqrt{\frac{1+e}{1-e}} \tag{3.15}$$

Figure 3.2 shows the resulting path of the orbitting body for various values of eccentricity. In each case the program was run to a final time of 20, corresponding to just over three orbits. We can see from the diagram that for each value of eccentricity the body follows the same elliptic path on each orbit. This behaviour is exactly what we would expect for this simple two-body problem.

3.2.1 Testing the Model

From figure 3.2 we can see that the program works, giving us an orbitting body following an elliptical path with one focus at the origin. However as discussed previously, a true test of its efficacy would be to look at the energy and the angular momentum. The calculation of each of these quantities was included at each time step of the program, so that a plot of their behaviour with time could be produced. Initially a time step of $h = 0.01$ was used. Figure 3.3a shows the behaviour of the energy, 3.3b the angular momentum.

From these we can see that there is no change of angular momentum as the time progresses, this is a good indication that the code is working. However there is a problem with the energy - the graph shows a periodic fluctuation after multiples of 2π, i.e. at the end of each orbit. This corresponds to the orbitting body passing the point of closest approach. Here, due to the effect of Kepler's second law, the speed is at its greatest value. This means that this area is modelled by fewer time steps, and thus we would expect a higher error due to the numerical scheme.

The fluctuations should disappear by reducing the step size to $h = 0.001$. An alternative way to improve the model would be to use variable step size, so that there is a smaller step when the velocity is greater [13]. This would perhaps be more efficient, however because the problem is relatively simple computation time is less of an issue. A variable step size would complicate the code unneccessarily therefore the problem will be solved by reducing h.

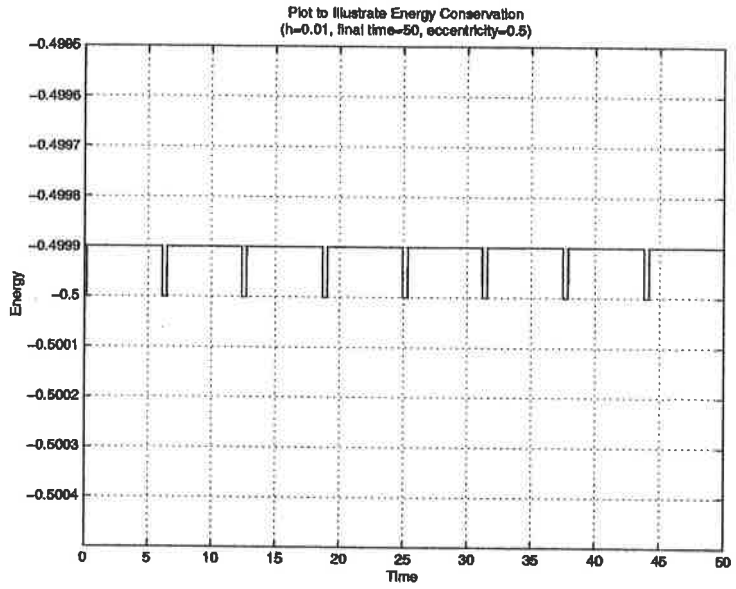

3.3a: Angular momentum versus time, $h = 0.01$, eccentricity= 0.5

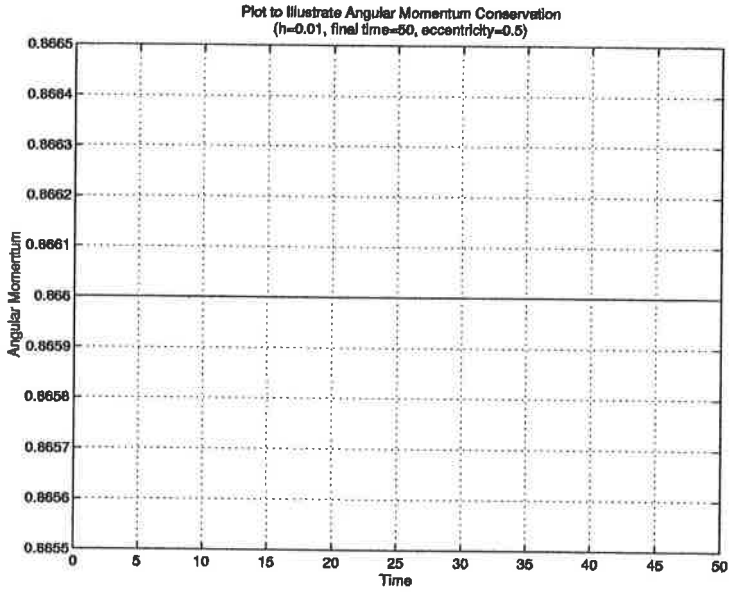

3.3b: Energy versus time, $h = 0.01$, eccentricity= 0.5

Figure 3.3: Behaviour of energy and angular momentum in the model

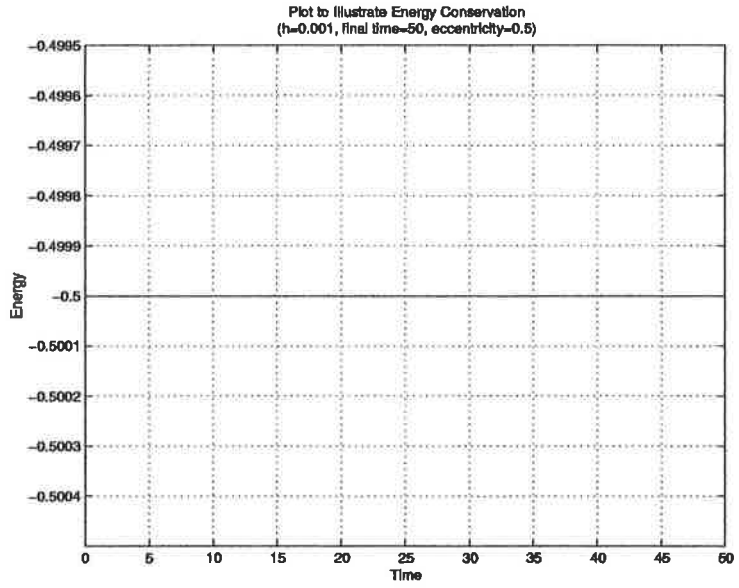

Figure 3.4: Energy versus time, $h = 0.001$, eccentricity$= 0.5$

Figure 3.4 shows the behaviour of the energy with the new value of h. This time we can see that the energy is constant over time. From these two experiments we can conclude that the model is a good representation of the two-body problem. However for all future work we will ensure that the step size remains at the smaller value to ensure that we have no problems relating to the discretisation.

3.2.2 Testing the Sensitivity

In the following chapters we shall often have to add a perturbation to the initial conditions. Before we can do this we need to see how sensitive the model is to the initial conditions. We would run in to difficulties later if the model required exactly those conditions given in equations (3.13) to (3.16) in order to give stable results. We have therefore run the non-linear model with

various perturbed initial conditions, given by $(\mathbf{Q}_0 + \delta\mathbf{Q}_0, \mathbf{P}_0 + \delta\mathbf{P}_0)$ where $(\mathbf{Q}_0, \mathbf{P}_0)$ is given by (3.13) to (3.16), and $(\delta\mathbf{Q}_0, \delta\mathbf{P}_0) = (\gamma\mathbf{Q}_0, \gamma\mathbf{P}_0)$, where γ is a scalar. We have also looked at the effect on ellipses with different values of the eccentricity.

The results of these tests are shown by figure 3.5. From this we can see that a stable ellipse is produced as long as the perturbation is sufficiently small. However we can also see that the eccentricity has an effect on the size of perturbation that can be tolerated. When we consider the example of a circle, shown in figure 3.5a, we can see that the model becomes unstable only if the perturbation reaches a similar magnitude as the original initial conditions. However, if we increase the eccentricity, as in figures 3.5b and 3.5c, we note that the results become unstable at a tenth of the unperturbed initial value, and this is more noticeable the higher the eccentricity of the ellipse. Note that the scales on these graphs vary, so that the ellipses do not look quite as they should, in particular figure 3.5a gives the results for the circle despite appearances. These results should not however cause a problem, as we shall mostly be working with smaller perturbations.

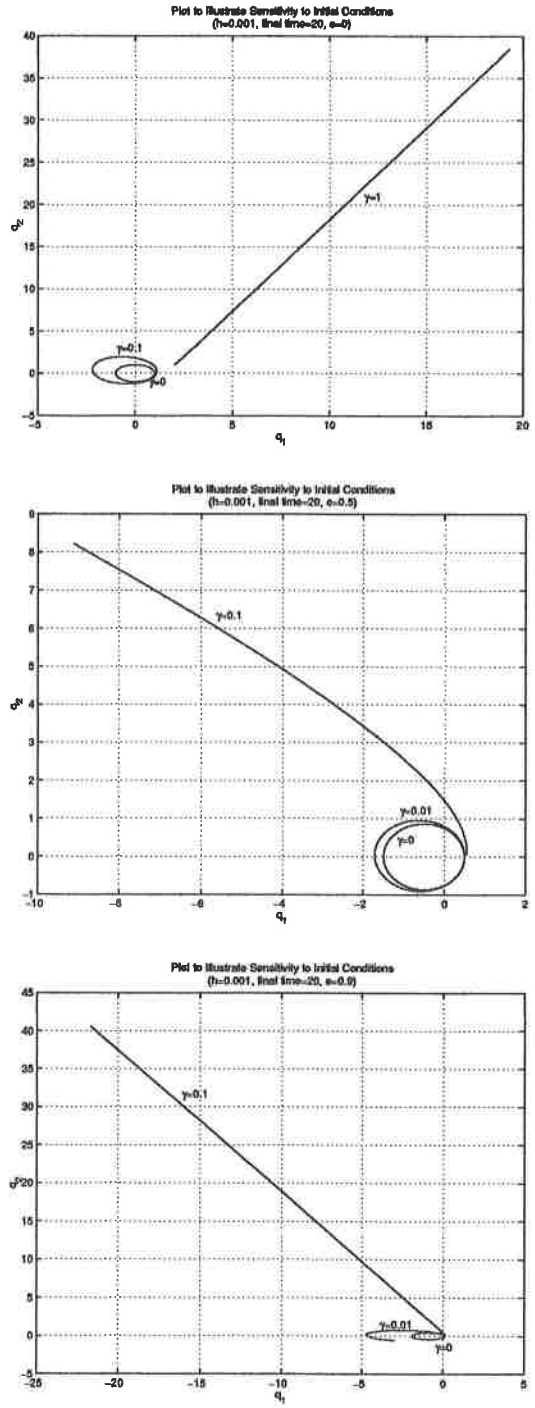

Figure 3.5: Graphs to show sensitivity to initial conditions for different eccentricities; a, $e = 0$; b, $e = 0.5$; c, $e = 0.9$

Chapter 4

Linearising Kepler's Problem

This chapter will discuss the linearisation of the numerical model, in order that we can test how well it conserves the global features. It is essential that the linearisation behaves correctly if we want to use a 4D-Var assimilation to input observational data into the model.

4.1 4D-Var Data Assimilation

Although we are not producing a complete 4D-Var assimilation scheme in this project, it is important that we understand why we are testing the linearisation. Much of the theory here is based on the lecture series by Bouttier and Courtier [2].

Data assimilation involves the integration of observations into a model to give a state that most accurately describes reality. However this is most frequently used in numerical weather prediction and there are often huge amounts of data, and also a huge state vector. A direct solution would in-

volve the inversion of a matrix that is too big to be achieved computationally. Data assimilation involves trying to find ways to approximate the problem to make it solvable. Variational methods do this by producing model states that most closely fit the observations and the background state, whilst obeying the model equations and retaining, if necessary, any physical constraints. They work by looking for the analysis which minimises a *cost function*, J. *4D-Var data assimilation* includes data that is distributed in time as well as space, its cost function is defined as

$$J(\mathbf{x}) = (\mathbf{x} - \mathbf{x}_b)^T \mathbf{B}^{-1} (\mathbf{x} - \mathbf{x}_b) + \sum_{n=0}^{N} (\mathbf{y}_n - H_n[\mathbf{x}_n])^T \mathbf{R}_n^{-1} (\mathbf{y}_n - H_n[\mathbf{x}_n]). \quad (4.1)$$

Here the subscript n denotes quantities at observation time n. $\mathbf{y}_n$ are the obsevations and $\mathbf{x}_n$ the model state, H_n is the observation operator, so that $\mathbf{y}_n - H_n[\mathbf{x}_n]$ is the innovation vector, describing the difference between the observations and the model state. The matrices $\mathbf{R}_n$ and $\mathbf{B}$ are the observation error and background error covariance matrices respectively.

The 4D-Var problem is defined as the minimization of (4.1) subject to the strong constraint that the model states, $\mathbf{x}_n$, are a solution of

$$\mathbf{x}_n = M_{0 \to n}(\mathbf{x}_0) \qquad \forall n, \quad (4.2)$$

where $\mathbf{x}_0$ is the initial state vector, and $M_{0 \to n}$ is the model operator that predicts the model state at time n from the initial conditions. Thus we have a non-linear constrained optimisation problem that is numerically dfficult to solve. In addition the minimisation algorithm is an iterative process that involves the calculation of the cost function *and* its gradient at *each* step.

The minimisation can be made simpler by making a series of assumptions.

- The observation operator H_n is linearized,
- Causality,
- Tangent linear hypothesis.

For the purposes of this project, the first of these approximations is not relevant. The remaining two, and in particularly the latter, are important in the linearization stage, and so I shall look at these in more detail.

4.1.1 Causality

This assumption requires that the model can be expressed as the product of intermediate model steps, reflecting the causality of nature. Usually this is the integration of a numerical model with given initial conditions, with n denoting observation time as before. The causality requirement is written mathematically as,

$$\mathbf{x}_n = M_n(M_{n-1}(\ldots(M_1(\mathbf{x}_0))\ldots)), \tag{4.3}$$

where M_n is the non-linear model acting at the n^{th} time step, and is defined such that $\mathbf{x}_i = M_i(\mathbf{x}_{i-1})$. If we consider our numerical model, we can see that it does obey the causality assumption. The new values of the position and momentum are found by applying the discretized model equations at each time step to the values from the previous step, starting with the initial conditions given in chapter 3.

We are therefore left to consider only the final assumption in our investigation into the linearisation of the two-body problem.

4.1.2 Tangent Linear Hypothesis

If we make the assumption that the model can be linearised, we find that the minimisation problem is simplified to an unconstrained quadratic problem that is far easier to solve. If we consider the Taylor expansion of a non-linear model, M, around state $\bar{\mathbf{x}}$, we thus have

$$M(\mathbf{x}+\delta\mathbf{x}) = M(\mathbf{x}) + M'(\mathbf{x})\delta\mathbf{x} + \frac{1}{2}M''(\mathbf{x})\delta\mathbf{x}^2 + \dots \tag{4.4}$$

The tangent linear hypothesis says that the model can be approximated by retaining only the linear terms, neglecting terms of higher order. Therefore if the linearisation is valid we have,

$$M(\mathbf{x}+\delta\mathbf{x}) = M(\mathbf{x}) + R(\mathbf{x})\delta\mathbf{x}, \tag{4.5}$$

where $R(\mathbf{x})$ is the linear model, defined by $R(\mathbf{x}) = M'(\mathbf{x})$.

Thus we can see that it is vital that the assumption is shown to be valid. If the linearization of the model does not retain the original features of the non-linear system, such as conservation properties, then the tangent linear hypothesis is not a good assumption, therefore the 4D-Var assimilation cannot be simplified. The aim of the remaining part of the project is to demonstrate that the Kepler problem *can* be successfully linearised, thus allowing the possibility of a 4D-Var scheme.

4.2 The Linear Model

We now need to produce the linear model of the two-body problem. To do this we need to consider again the equations of motion discussed in Chapter 2.

Recall the non-dimensionalised, canonical form.

$$\frac{\mathrm{d}\mathbf{q}}{\mathrm{d}t} = \mathbf{p} \tag{4.6}$$

$$\frac{\mathrm{d}\mathbf{p}}{\mathrm{d}t} = -\frac{\mathbf{q}}{(q_1^2+q_2^2)^{\frac{3}{2}}} \tag{4.7}$$

These describe the time evolution of position and momentum. Now, if we consider the time evolution of a general state vector, $\mathbf{x}$, we thus have

$$\frac{\mathrm{d}\mathbf{x}}{\mathrm{d}t} = F(\mathbf{x}). \tag{4.8}$$

After discretisation, we have numerical model M, such that

$$\mathbf{x}(t) \to \mathbf{x}(t+T) = M(t+T,t)\mathbf{x}(t). \tag{4.9}$$

We linearise around $\bar{\mathbf{x}}$ which is a solution of equation (4.8), i.e. we substitute $\mathbf{x} = \bar{\mathbf{x}} + \delta\mathbf{x}$ into the model, and drop non-linear terms. We can then find the tangent-linear equation [14],

$$\frac{\mathrm{d}\delta\mathbf{x}}{\mathrm{d}t} = F'_{\mathbf{x}(t)} \cdot \delta\mathbf{x}, \tag{4.10}$$

where $F'(\mathbf{x})$ is the Jacobian of $F(\mathbf{x})$ with respect to state vector $\mathbf{x}(t)$. This describes the evolution of the perturbation, to first order, in the vicinity of trajectory $\mathbf{x}(t)$.

We then discretise to find the tangent linear model R

$$\delta\mathbf{x}(t) \to \delta\mathbf{x}(t+T) = R(t+T,t)\delta\mathbf{x}(t). \tag{4.11}$$

If we consider our system of equations, we can thus find the linear equations by differentiating equations (4.6) and (4.7). The resulting non-dimensional equations governing the evolution of the perturbation are,

$$\frac{\mathrm{d}\delta\mathbf{q}}{\mathrm{d}t} = \delta\mathbf{p} \tag{4.12}$$

$$\frac{\mathrm{d}\delta\mathbf{p}}{\mathrm{d}t} = -\frac{\delta\mathbf{q}}{(q_1^2+q_2^2)^{\frac{3}{2}}} + \frac{3\mathbf{q}(q_1\delta q_1 + q_2\delta q_2)}{(q_1^2+q_2^2)^{\frac{5}{2}}} \tag{4.13}$$

These are then discretised using the same numerical scheme, the Störmer-Verlet method, as for the non-linear model. Note that in practice we linearise the discrete numerical non-linear model, rather than disretise the linearised model. There are some cases where this distinction is important [9], however in this example the result is the same. We then have our tangent linear model,

$$\delta\mathbf{P}_{n+\frac{1}{2}} = \delta\mathbf{P}_n - \frac{h}{2}\frac{\delta\mathbf{Q}_n}{(Q_{1n}^2+Q_{2n}^2)^{\frac{3}{2}}} + \frac{h}{2}\frac{3\mathbf{Q}_n(Q_{1n}\delta Q_{1n}+Q_{2n}\delta Q_{2n})}{(Q_{1n}^2+Q_{2n}^2)^{\frac{5}{2}}} \tag{4.14}$$

$$\delta\mathbf{Q}_{n+1} = \delta\mathbf{Q}_n + h\delta\mathbf{P}_{n+\frac{1}{2}} \tag{4.15}$$

$$\delta\mathbf{F}_{n+1} = -\frac{\delta\mathbf{Q}_{n+1}}{(Q_{1n+1}^2+Q_{2n+1}^2)^{\frac{3}{2}}} + \frac{3\mathbf{Q}_{n+1}(Q_{1n+1}\delta Q_{1n+1}+Q_{2n+1}\delta Q_{2n+1})}{(Q_{1n+1}^2+Q_{2n+1}^2)^{\frac{5}{2}}} \tag{4.16}$$

$$\delta\mathbf{P}_{n+1} = \delta\mathbf{P}_{n+\frac{1}{2}} + \frac{h}{2}\delta\mathbf{F}_{n+1} \tag{4.17}$$

Here $\delta\mathbf{Q}_n$ and $\delta\mathbf{P}_n$ are the position and momentum perturbations respectively at time level n. The vectors $\mathbf{Q}_n$ and $\mathbf{P}_n$ are found using the unperturbed non-linear model.

4.2.1 Testing the Linear Model

In order to test the *code*, we need to check that the tangent-linear model is the correct linearisation of the non-linear model in the vicinity of a given trajectory. Consider a general state variable $\mathbf{x}$, and perturbation $\delta\mathbf{x}$. From equation (4.4) we have,

$$\frac{M(\mathbf{x}+\delta\mathbf{x})_i - M(\mathbf{x})_i}{[R(\mathbf{x})\delta\mathbf{x}]_i} = 1 + \text{higher order terms}, \tag{4.18}$$

where M is the non-linear model for two different initial conditions, R is the tangent-linear model describing the evolution of the perturbation, and the subscript i denotes the i^{th} vector component. As we have seen the tangent linear model is valid only if higher order terms are negligible, therefore if we take the limit as $\delta\mathbf{x}$ tends to zero of the right-hand side and subtract one then the answer should tend to zero, as shown in the following equation.

$$\lim_{\mathbf{x}\to 0} \frac{M(\mathbf{x}+\delta\mathbf{x})_i - M(\mathbf{x})_i}{[R(\mathbf{x})\delta\mathbf{x}]_i} - 1 = 0. \tag{4.19}$$

In addition, this limit should be reached linearly, proving that the linear part of the Taylor series is explained by the tangent-linear model. This is known as testing the *correctness* of the model [14].

To carry out this test on the numerical model, we need to run the non-linear model twice, once with initial conditions $(\mathbf{Q}_0, \mathbf{P}_0)$, as given by equations (3.13) to (3.16) then with $(\mathbf{Q}_0 + \delta\mathbf{Q}_0, \mathbf{P}_0 + \delta\mathbf{P}_0)$. We also need to run the tangent-linear model with initial perturbation vector $(\delta\mathbf{Q}_0, \delta\mathbf{P}_0) =$

$(\gamma \mathbf{Q}_0, \gamma \mathbf{P}_0)$, where γ is a scalar. We are then able to calculate the left-hand side of equation (4.19) for decreasing values of the initial perturbation. In the model we run the model for eight initial perturbations, with γ decreasing by a factor of ten each time. The graphs of perturbation versus the value found for the left-hand side, which we refer to as the error, have been plotted using a logarithmic scale on both axes.

Figure 4.1 shows the graphs for three different values of the eccentricity, $e = 0$, $e = 0.5$, and finally $e = 0.9$. Each was run to a final time, $t = 20$, where the time is in the non-dimensionalised unit described in chapter 2. We can see from these that in all three cases there is a definite tendency to zero to the limits of computer accuracy, and this does occur linearly. However, there is a noticeable difference between the three graphs. The circle ($e = 0$) produces the best results, tending towards a smaller number for the smallest value of γ, and behaving more linearly for larger γ than the higher eccentricity examples. Thus giving the idea that the higher the eccentricity, the more non-linear the behaviour of the Kepler problem.

Figure 4.2 gives correctness graphs for various lengths of model run, $t = 5$, t=20, $t = 50$. We can see that for a shorter run time, there is a tendency towards a smaller value for the error at lower γ values, and the behaviour is more linear for larger initial perturbations. The longer the run time, the less linear the behaviour for larger γ and for small γ the error is larger than with a shorter run. This is as we would expect, as any errors due to linearisation would become magnified with time.

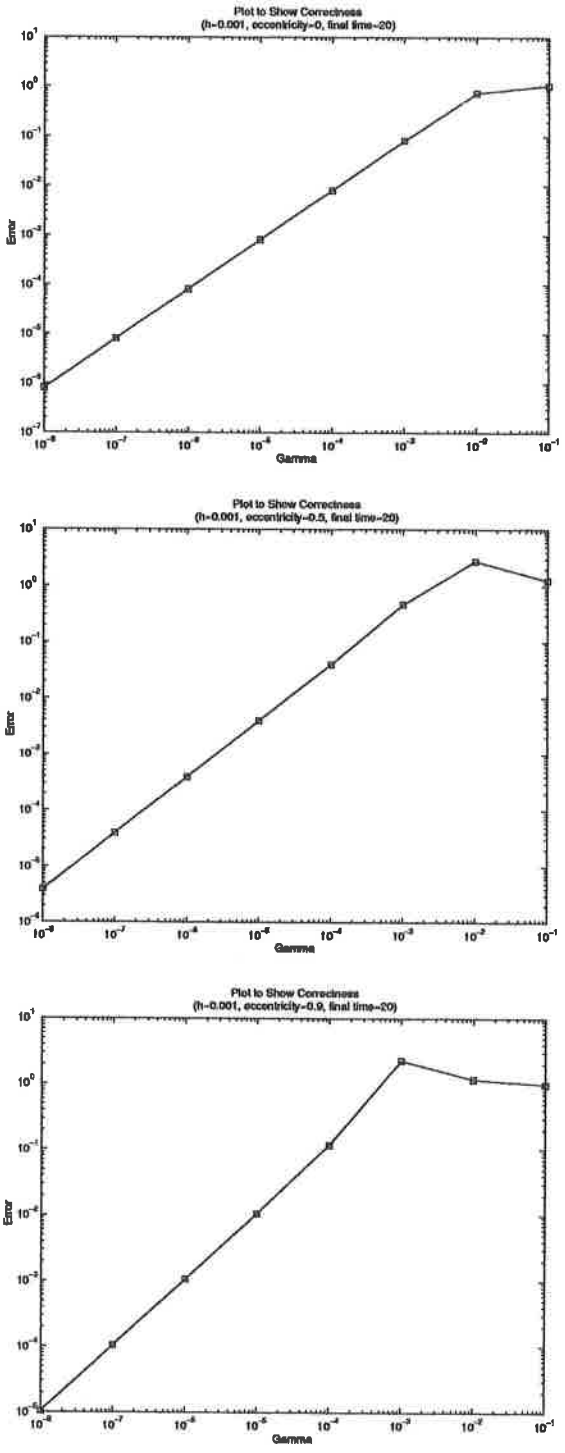

Figure 4.1: Graphs to Illustrate Correctness for Various Eccentricities

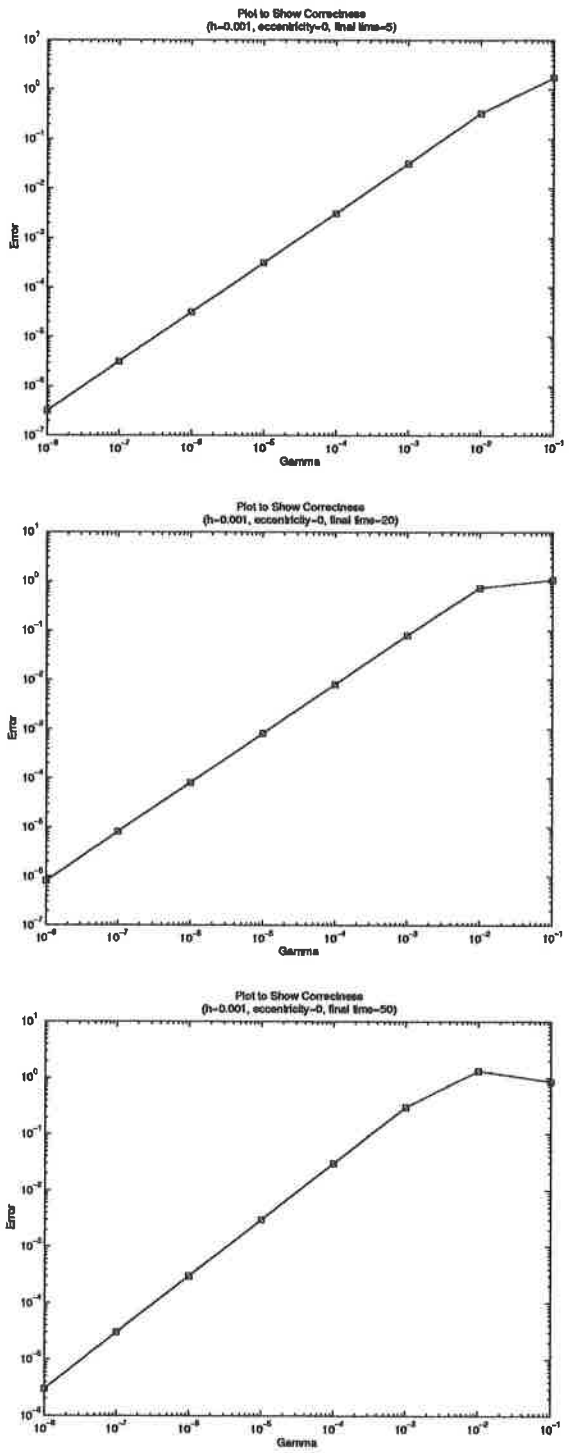

Figure 4.2: Graphs to Illustrate Correctness for Various Run Times

From these tests we can see that the tangent-linear model code is correct. Even for the longer runs, or larger eccentricities, the linear tendency towards zero is pronounced enough to reach this conclusion. We are now able to carry on and see if the linear model is a good approximation for the non-linear problem, and whether it conserves the global properties.

Chapter 5

Numerical Experiments

We have found that the code for our linear model of the two-body problem is correct. However this does not neccessarily mean that the tangent linear hypothesis holds for this problem, we need to do some further tests.

5.1 Validity

The validity of the model is the length of time under which the linear model is a good approximation of the non-linear problem. There are of course errors associated with linearisation, and these will increase as time progresses. The model is valid only where the linear model mirrors the behaviour to a reasonable degree of accuracy of the original problem. To do this, we need to track the evolution of a perturbation in both of our models. We run the non-linear model with two sets of initial conditions, $(\mathbf{Q}_0, \mathbf{P}_0)$ and $(\mathbf{Q}_0 + \delta\mathbf{Q}_0, \mathbf{P}_0 + \delta\mathbf{P}_0)$, where vectors $\mathbf{Q}_0$ and $\mathbf{P}_0$ are the same initial conditions as listed in equations (3.13) to (3.16), and the initial perturbations, $(\delta\mathbf{Q}_0, \delta\mathbf{P}_0)$, are as described in section 4.2.1. The same initial perturbation is used as the initial con-

ditions for the tangent linear model, this also uses the data from the first, unperturbed run of the non-linear model as the linearisation state. We then compare the result of the tangent linear model, which returns values for $\delta\mathbf{Q}$ and $\delta\mathbf{P}$ at each time step, with the difference in position and momenta produced by the two model runs of the non-linear scheme. The validity time is thus the point at which the non-linear and linear model results begin to separate greatly. We have done this for various sizes of γ and eccentricity. The graphs below show only the results for the Q_1 component in most cases, however we include the graph of the P_1 component for $\gamma = 0.01$, $e = 0$ (see figure(5.3)), to illustrate that the other vector components behave in a very similar manner.

Figure 5.1 illustrates the effect of changing the size of the perturbation, whilst keeping the eccentricity fixed, $e = 0$. We show the results for $\gamma = 0.1$, $\gamma = 0.01$ and $\gamma = 0.001$ respectively. The solid line indicates the results given by the non-linear model, the dashed line those produced by the tangent linear model. These graphs confirm that the validity time is longer for smaller perturbations. This is as we would expect, the smaller the size of the perturbation, the smaller the size of the non-linear components that have been neglected in the linear model.

Figure 5.2 shows how changing the eccentricity effects the validity, whilst fixing $\gamma = 0.01$. We use this value of γ because it is large enough to observe differences in behaviour due to the change in eccentricity, but small enough to avoid the possible instabilities we noticed in figure 3.5.

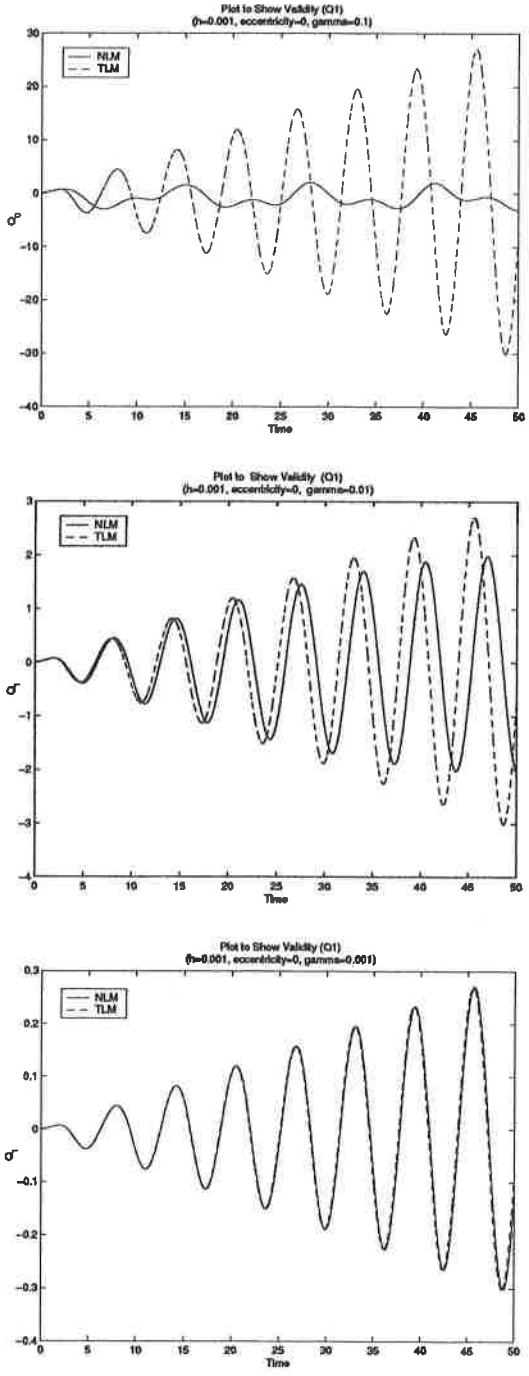

Figure 5.1: Evolution of the Q_1 perturbation for the non-linear and linear models, for different γ ($h = 0.001$, $e = 0$, $\gamma = 0.1, 0.01, 0.001$)

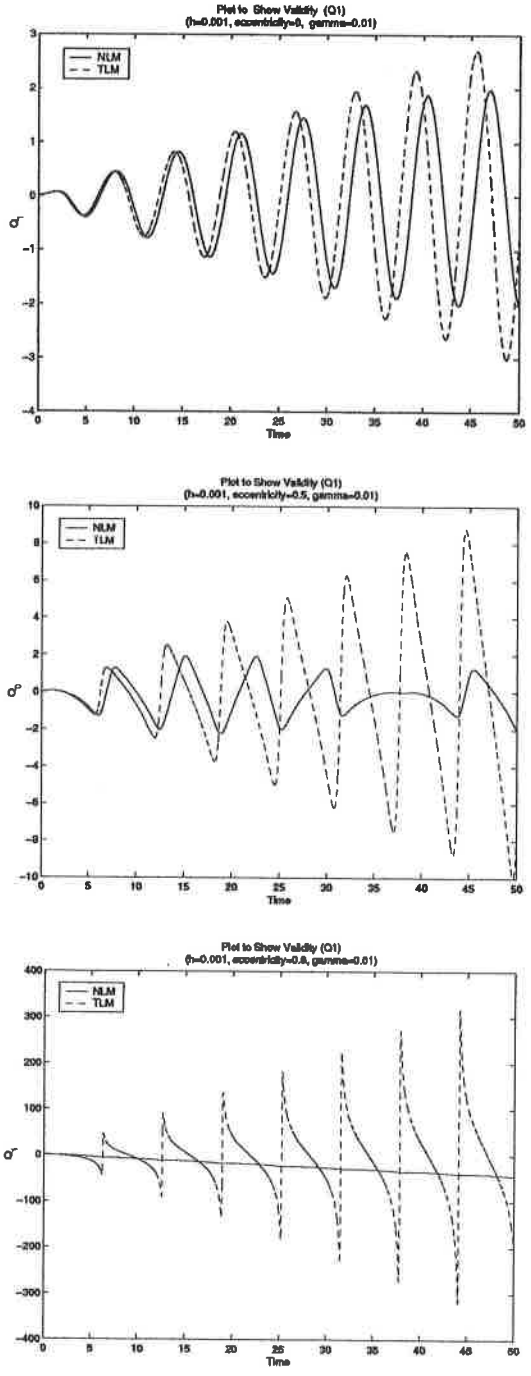

Figure 5.2: Evolution of the Q_1 perturbation for the non-linear and linear models, for different eccentricities ($h = 0.001$, $\gamma = 0.01$, $e = 0, 0.5, 0.9$)

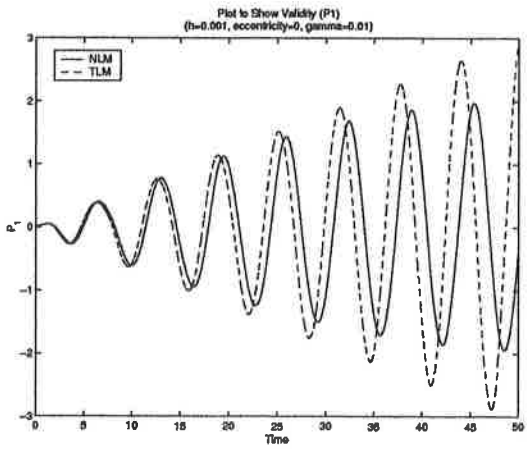

Figure 5.3: Evolution of the P_1 perturbation for the non-linear and linear models, for different γ ($h = 0.001$, $e = 0$, $\gamma = 0.01$)

We have shown the results for $e = 0$, $e = 0.5$ and $e = 0.9$. From these we see that the validity time is shorter for larger eccentricities. For $e = 0$, the two models exhibit similar behaviour, and the validity time is long. However for $e = 0.5$, the linear model stops being a good representation for the non-linear model after only two orbits, after this the behaviour becomes increasingly different as the perturbations evolve. This is exaggerated further for $e = 0.9$, here the linear model departs from the non-linear almost immediately, and produces unstable results. This qualitative relationship between validity time and eccentricity backs up the results found in chapter 4, giving further evidence that more eccentric ellipses exhibit more non-linear behaviour.

Figure 5.3 illustrates the evolution of the $\mathbf{P}_1$ component in both the non-linear and linear models. By comparison with figure 5.1b, we can see that the position and momentum perturbations behave in a very similar manner.

5.2 Conservation Properties

We have discussed throughout this report that one of the most important features of this problem is its energy and angular momentum conservation properties. We may wish to use these conservation laws in order to introduce observations into a 4D-Var assimilation scheme. For example, we may accurately know the position of the orbitting body but not its momentum. The two conservation laws would then allow us to find the momentum and include it in the assimilation. However this will only be accurate if the linear model retains the same conservation properties. In order to carry out this test we need to linearise the energy and momentum equations.

Recall equations (2.17) and (2.18), energy is given by

$$E = \frac{1}{2}\left(p_1^2 + p_2^2\right) - \frac{1}{(q_1^2 + q_2^2)^{\frac{1}{2}}} = \text{constant}, \tag{5.1}$$

angular momentum by

$$L = q_1 p_2 - p_1 q_2 = \text{constant}. \tag{5.2}$$

In thisOnce linearised and discretised, the expression for the linearised energy is as follows,

$$P_1 \delta P_1 + P_2 \delta P_2 + \frac{Q_1 \delta Q_1 + Q_2 \delta Q_2}{(Q_1^2 + Q_2^2)^{\frac{3}{2}}} = \text{constant}, \tag{5.3}$$

and for the angular momentum we have

$$\delta Q_1 P_2 - P_1 \delta Q_2 + Q_1 \delta P_2 - \delta P_1 Q_2 = \text{constant}. \tag{5.4}$$

The equations above are found by linearising around $\bar{\mathbf{q}}$ and $\bar{\mathbf{p}}$. We can also find non-linear expressions for the energy perturbations, obtained by calculating,

$$\delta E = E(\bar{\mathbf{q}} + \delta\mathbf{q}, \bar{\mathbf{p}} + \delta\mathbf{p}) - E(\bar{\mathbf{q}}, \bar{\mathbf{p}}), \tag{5.5}$$

where E is the non-linear expression for energy given by (5.1). We can find a similar expression for the non-linear angular momentum perturbation.

We can now do four different tests, looking at the behaviour of the energy only. We will later include an example of the angular momentum to show it behaves in a similar manner. We will be investigating the two different expressions for the energy perturbation, the linear expression for δE given by (5.3) which we shall refer to as E_{Lin}, and the non-linear expression, E_{NL}, given by (5.5).

We again carry out two non-linear model runs, with the same two sets of initial conditions as described in section 5.1. This gives us our non-linear perturbations for the position and momentum. We also run the linear model to find the linear position and momentum perturbations. We can thus investigate the behaviour of E_{NL} with both the non-linear and linear perturbations, and E_{Lin} for both sets of data, thus giving us our four tests.

Figures 5.4 to 5.6 show the results for the energy for different eccentricities, $e = 0$, $e = 0.5$, $e = 0.9$, fixing $\gamma = 0.001$. Each figure is split into a and b. Figure a shows E_{NL} with the non-linear data and E_{Lin} with the linear data, b shows the results from all four of the tests.

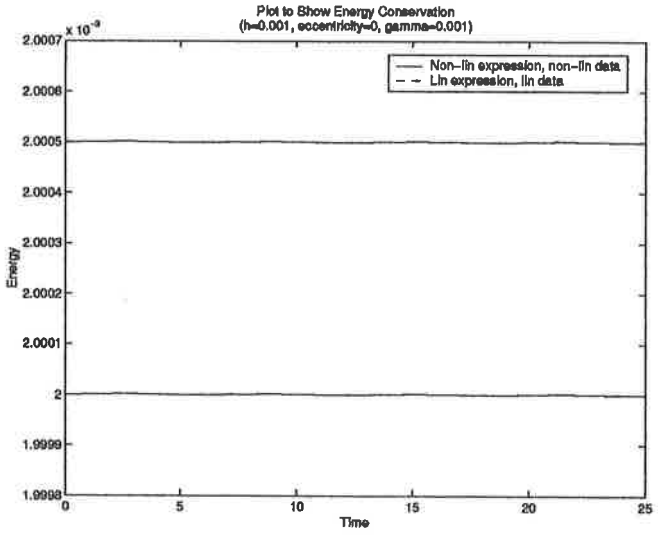

Figure 5.4a

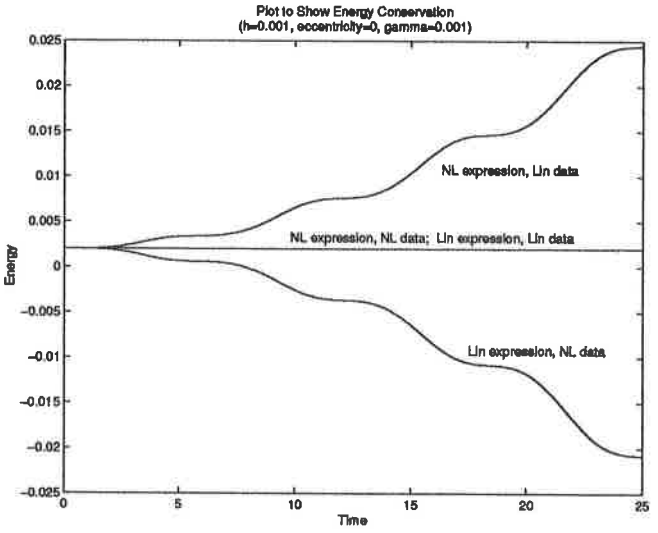

Figure 5.4b

Figure 5.4: Non-linear and linear expressions for the energy, $h = 0.001$, $e = 0$, $\gamma = 0.001$

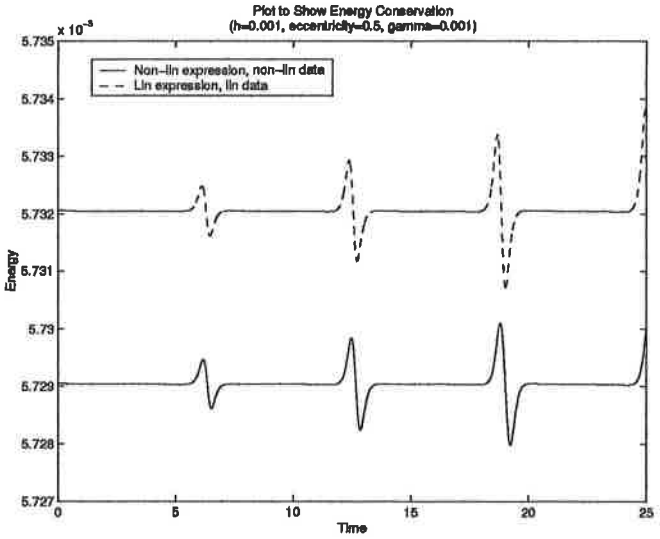

Figure 5.5a

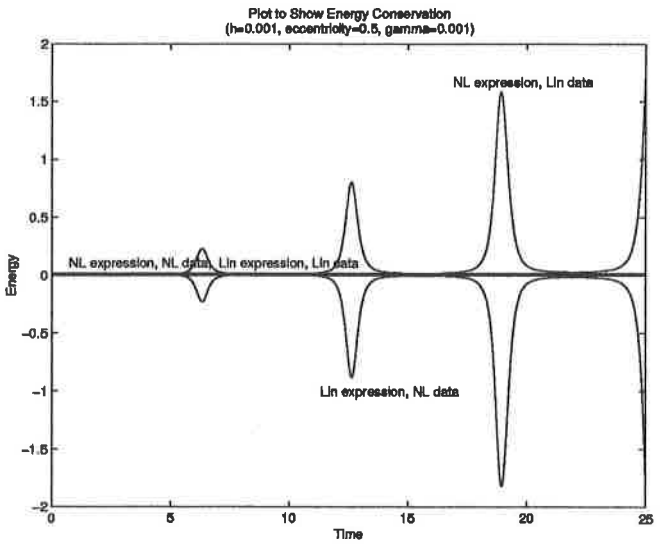

Figure 5.5b

Figure 5.5: Non-linear and linear expressions for the energy, $h = 0.001$, $e = 0.5$, $\gamma = 0.001$

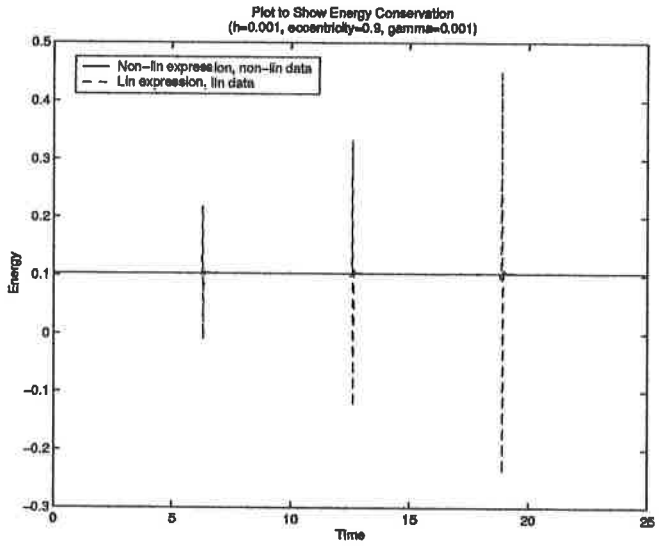

Figure 5.6a

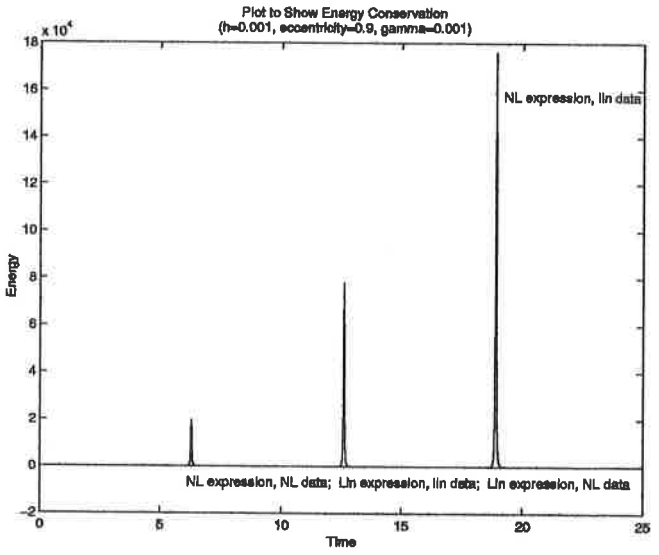

Figure 5.6b

Figure 5.6: Non-linear and linear expressions for the energy, $h = 0.001$, $e = 0.9$, $\gamma = 0.001$

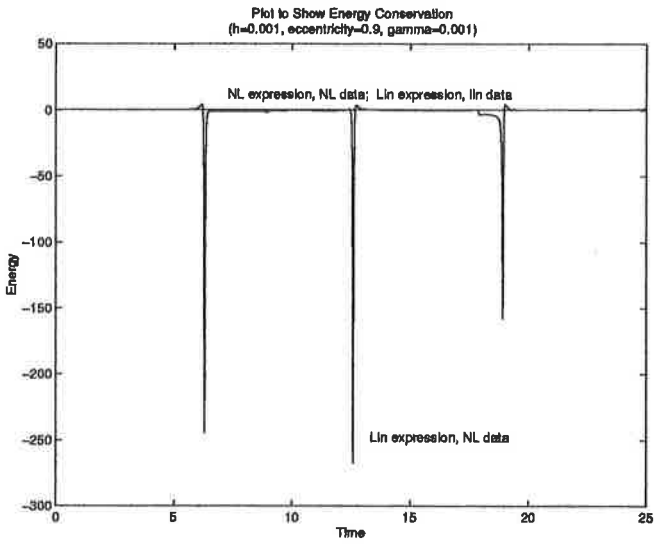

Figure 5.7: Non-linear and linear expressions for the energy, $h = 0.001$, $e = 0.9$, $\gamma = 0.001$

Because the non-linear energy expression with the linear data swamps figure 5.6b, figure 5.7 does not include this so that we can distinguish the behaviour of the linear model with the non-linear data. Figure 5.7 shows the evolution of the energy perturbation as given by E_{Lin} with the non-linear data.

We initially consider the results for the circle, shown in figure 5.4. Figure 5.4a shows the behavior of E_{NL} with the non-linear perturbations, and E_{Lin} with the linear data. We can see that these behave as we would expect, they remain constant in time with values very close to zero and the difference between them is negligible. When we include E_{NL} with the linear data, and E_{Lin} with the non-linear perturbations, we can see that they behave in a very similar manner, both diverge from the constant line, and at a similar rate.

This is because the linear and non-linear perturbations are almost identical, as we can see in figure 5.1.

When we consider figure 5.5, with $e = 0.5$, we notice that the behaviour is different. If we consider figure 5.5a, we notice that the energy perturbations are no longer constant in time. There is a fluctuation occurring after multiples of 2π, i.e at the perihelion, this could be the beginning of an instability due to the discretisation. When we carried out the test of energy conservation in our non-linear model (see section 3.2.1) we were looking at the energy, here we are considering the energy *perturbation*, thus the numbers are of a smaller magnitude. Thus we may now be seeing a problem with the discretisation which was not previously apparent.

When we look at figure 5.5b, we can see that again E_{NL} with the linear data and E_{Lin} with the non-linear, diverge from the constant line. This time however E_{NL} with the linear data moves away at a slower rate, suggesting that the errors due to linearisation are worse when linearising the expression for energy, than when linearising the actual model. The peaks that are observed here are probably due to the fluctuations in figure 5.5a, and indicate that perhaps there is an instability.

Figures 5.6 and 5.7 illustrate the results for $e = 0.9$. By looking at the y-axis scale we can see that the system has become unstable. If we consider figure 5.2, we had already observed instabilities associated with this highly eccentric orbit. Figures 5.6 and 5.7 are likely to be a result of this behaviour.

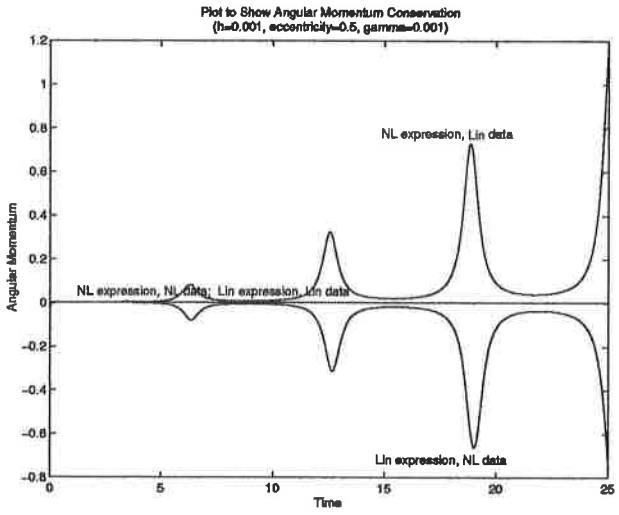

Figure 5.8: Non-linear and linear expressions for the angular momentum, $h = 0.001$, $e = 0.5$, $\gamma = 0.001$

Although there were problems with large eccentricities, we can still consider the circle when looking at the conservation properties. From this we can see that we would have to be cautious when considering the possibility of using the conservation laws to incorporate observations into a 4D-Var scheme. To do this we would probably want to put linearised data into the system using E_{NL}. Our results show this is not a conserved quantity, and that we would be *adding* energy to the system, thus destroying the conservation of energy within the non-linear model.

As the behaviour for the angular momentum is very similar to the for energy, we have not included extensive results. However figure 5.8 illustrates this similar behaviour by showing the angular momentum perturbation evolution for all four tests, with $e = 0.5$. We can see by comparing this figure

to figure 5.5b, that although the angular momentum perturbation peaks are slightly smaller, they occur at the same time as the energy perturbation peaks.

Chapter 6

Conclusion

To conclude we shall discuss the success of the various stages in setting up the linear model. We began by producing a numerical scheme to model the non-linear equations of motion. The Störmer-Verlet method was decided upon, and this second order Runge-Kutta scheme proved to be a good choice, successfully conserving both angular momentum and energy once the step size, h, was made sufficiently small.

We then went on to linearise this model, in order to investigate whether the Kepler problem could be successfully linearised. We carried out correctness tests on the code to show that it was working. These tests behaved exactly as we would expect, as the initial perturbation decreased in size, we noticed that the linear model and non-linear model values converged, and that this happened linearly. We thus concluded that the code was correct, and we could look at the viability of the linearisation.

The next test involved looking at the validity time, this is the period over

which the linear model is a good representation of the non-linear model. To do this we compared the evolution of the perturbations in each case. We looked at the effect of changing the size of the initial perturbation, and found, as expected, that the smaller this initial perturbation, the longer the two models coincided. This again confirms that the linear model is correct. We then went on to investigate the effect of changing the eccentricity. We noticed that the validity time for the case of a circle was much longer, and that even at later times, after several completed orbits, the linear model behaviour was still similar to that of the non-linear model. However as the eccentricity increased, the validity time decreased, and for highly eccentric orbits instabilities were observed. Thus we can see that the non-linear components of the Kepler problem become larger as the eccentricity increases.

Finally we looked at four different cases for energy conservation, E_{NL} using both the non-linear and linear perturbations, and E_{Lin} with the two different sets of data. We noticed that for a circle, the two expressions for energy were conserved if their appropriate data was used, although the two values differed slightly. However if the opposite data (e.g. E_{NL} with the linear perturbations) was used the energy begins to diverge, for a circle the magnitude of the divergence is similar because the linear and non-linear pertrubations are of a comparable size. As we increased the eccentricity, the divergence was greater, and we began to notice fluctuations in the results, indicating possible instabilities. For highly eccentric orbits the problem became unstable. This is possibly a result of discretisation, and could possibly be overcome by implementing a variable step size scheme. This would allow the region around

the perihelion to be modelled by a greater number of steps, thus improving the model accuracy.

We can see from this that although the Kepler problem can be successfully linearised, particularly for more circular orbits, we must still be cautious when considering the use of the conservation laws to incorporate data into an incremental 4D-Var scheme. Were these to be used, we may destroy the conservation properties of the non-linear model, and add energy into the system.

Bibliography

[1] David Acheson: *From Calculus to Chaos, An Introduction to Dynamics*, Oxford University Press, 1997

[2] F. Bouttier and P. Courtier: *Data assimilation concepts and methods*, ECMWF Meteorological Training Course Lecture Series, March 1999

[3] C. J. Budd and M. D. Piggott: *Geometric Integration and Its Applications*, from the proceedings of the ECMWF Workshop on Developments in numerical methods for very high resolution global models, 5-7 June 2000, 93-117

[4] Winston C. Chao and Lang-Ping Chang: *Development of a Four-Dimensional Variational Analysis System Using the Adjoint Method at GLA. Part1: Dynamics*, Monthly Weather Review, August 1992, 1661-1673

[5] Philippe Courtier and Olivier Talagrand: *Variational assimilation of meteorological observations with the direct and adjoint shallow-water equations*, Tellus (1990), 42A, 521-549

[6] P. Coutier, J-N Thépault and A. Hollingsworth: *A Strategy for Operational Implementation of 4D-Var, Using an Incremental Approach*, Q. J. R. Meteorol. Soc, 120, 1367-1387

[7] Anne K. Griffith and N. K. Nichols: *Data Assimilation Using Optimal Control Theory*, Numerical Analysis Report October 1994, University of Reading

[8] E. Hairer: *Numerical geometric integration*, Lecture notes (1999), University of Geneva, see www.unige.ch/math/folks/hairer

[9] Amos Lawless: *Development of Linear Models for Data Assimilation in Numerical Weather Prediction*, PhD thesis, May 2001, Dept of Mathematics, University of Reading

[10] François-Xavier Le Dimet and Olivier Talagrand: *Variational algorithms for analysis and assimilation of meteorological observations: theoretical aspects*, Tellus (1986), 38A, 97-110

[11] Dean Parry: *Construction of Symplectic Runge-Kutta Methods and their Potential for Molecular Dynamics Applications*, MSc thesis, September 1997, Dept of Mathematics, University of Reading

[12] J. M. Sanz-Serna and M. P. Calvo: *Numerical Hamiltonian Problems*, Chapman and Hall, 1994

[13] Robert D. Skeel and Jeffrey J. Biesiadecki: *Symplectic Integration with Variable Stepsize*, Annals of Numerical Mathematics 1 (1994) 1-9

[14] Jean-Noël Thépault and Philippe Courtier: *Four-dimensional variational data assimilation using the adjoint of a multilevel primitive equation model*, Q. J. R. Meteorol. Soc. (1991), 117, 1225-1254